Well-Defined Precision Ethylene/Vinyl Fluoride Polymers: Synthesis and Crystalline Properties

Emine Boz, Alexander J. Nemeth, and Kenneth B. Wagener*

The George and Josephine Butler Polymer Research Laboratory and Center for Macromolecular Science and Engineering, Department of Chemistry, University of Florida, Gainesville, Florida 32611-7200

Keesu Jeon,[†] Robert Smith,[†] Farhod Nazirov,[†] Michael R. Bockstaller,[‡] and Rufina G. Alamo*,[†]

Department of Chemical and Biomedical Engineering, FAMU/FSU College of Engineering, Tallahassee, Florida 32310-6046, and Department of Materials Science and Engineering, Carnegie Mellon University, Pittsburgh, Pennsylvania 15213

Received June 24, 2007; Revised Manuscript Received November 20, 2007

ABSTRACT: Here we report the synthesis and crystalline structure of a family of three precision ethylene/vinyl fluoride (EVF) polymers with fluorine atoms on each and every 9th, 15th, and 21st carbon via ADMET polymerization, followed by exhaustive hydrogenation. The primary structure of the polymers is confirmed by NMR, TGA, IR, and elemental analysis. The crystallization pattern of these systems is analogous to that of homopolymers as evidenced by the equivalent halogen content in amorphous and crystalline regions, as obtained by solid-state NMR. This is supported by SAXS periodicities that conform with layered crystalline−amorphous structures of folded chains. While the thickness of the amorphous layer is small (∼45 Å) and constant within the series, the crystallite thicknesses (∼200−100 Å) decrease with increasing fluorine. The latter, and the depression of crystallinity, equilibrium melting, and heat of fusion with increasing content of F attest to the restrictions of this halogen, although of a small volume, as a defect to the crystallization of these systems. Nonetheless, strain from the inclusion of the fluorine atom in the crystal lattice of the three precision EVF polymers investigated is small, such that the orthorhombic packing of the polyethylene chain is maintained in these new polymers.

Introduction

Fluoropolymers are industrially important materials that find application in areas where thermal and chemical resistance are critical to performance.[1] As the first and most well-known fluoropolymer, poly(tetrafluoroethylene) (PTFE or Teflon) finds numerous applications in household, industrial, and aerospace settings.[2] While PTFE is a fully fluorinated polyethylene (PE) analogue, numerous partially fluorinated analogues are also known and used commercially in a variety of applications. Among the most well-known partially fluorinated polymers are poly(vinyl fluoride) (PVF), poly(vinylidene fluoride) (PVDF), poly(ethylene tetrafluoroethylene) (PETFE), and random ethylene vinyl fluoride (EVF) polymers.[3,4] In all such polymers, a variation in properties is achieved via the tuning of the fluorine content as well as the distribution of hydrogens and fluorines in the backbone.[3]

In an attempt to correlate properties with polymer composition in these partially fluorinated polymers, the presence of defects within the polymer backbones must be taken into account. Common defects include head-to-head and tail-to-tail linkages and chain branching.[4] In order to fully correlate fluorine content with physical properties, a family of well-defined and defect free partially fluorinated polymers is required. Herein we present a family of precision EVF polymers with a fluorine atom on each and every 9th, 15th, and 21st carbon, synthesized using acyclic diene metathesis (ADMET) polymerization followed by hydrogenation. The primary chain characterization and melting and crystalline properties are analyzed in reference to the unsubstituted polyethylene chain. In addition to providing the means of studying the properties of EVF polymers, characterization of this family of precision EVF polymers provides a comparison to the previously reported precision ethylene/vinyl chloride[5] (EVC) and precision ethylene/vinyl bromide[6] (EVB) polymers with matched compositions. Therefore, a comparison of the apparent melting behavior based not only on halogen content but also on halogen size is also presented.

Results and Discussion

Monomer and Polymer Synthesis. Synthesis of the necessary fluorinated α−ω-diene monomers is illustrated in Scheme 1. The alcohol precursors (**4**−**6**) were prepared as described earlier.[6] Conversion of the alcohols to the corresponding fluorine monomers (**7**−**9**) was realized by reaction with DAST ((diethylamino)sulfur trifluoride). Polymerization was carried out in toluene at 45 °C with Grubbs' first-generation ruthenium

Scheme 1

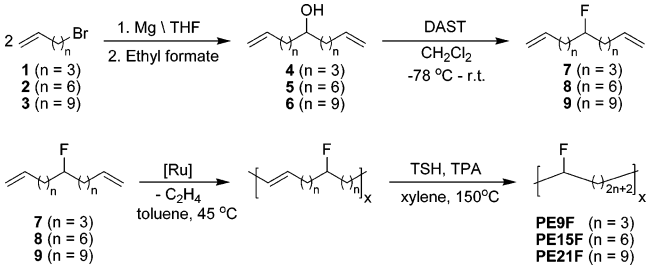

* Corresponding authors. E-mail: wagener@chem.ufl.edu; alamo@eng.fsu.edu.
[†] FAMU/FSU College of Engineering.
[‡] Carnegie Mellon University.

10.1021/ma071403n CCC: $40.75
Published on Web 02/06/2008

Table 1. Molar Mass and Thermal Data of Linear Polyethylenes and Precision EVFs

sample	$M_w \times 10^3$	M_w/M_n	T_m (°C)	T_c (°C)	ΔH_f (J/g)	X_c[b]	first stage onset of decomposition[c] (°C)	second stage onset of decomposition[d] (°C)
ADMET PE	16.0[a]	1.6	130	114	260	88	348	384
PE21F	7.6[a]	1.8	124	113	205	74	294	418
PE15F	10.4[a]	2.2	124	114	174	64	257	410
PE9F	8.9[a]	2.0	123	114	137	53	210	408

[a] GPC vs PE in DCB. [b] Percent crystallinity (X_c) from heat of fusion in reference to the value of fully crystalline polyethylene, 985 cal/mol[9] (for uniform distribution of F, this value translates into 276 J/g for **PE21F**, 270 J/g for **PE15F** and 256.5 J/g for **PE9F**). [c] Recorded at first stage 5% total mass loss under nitrogen gas, 10 °C/min. [d] Recorded at second stage 10% total mass loss under nitrogen gas, 10 °C/min.

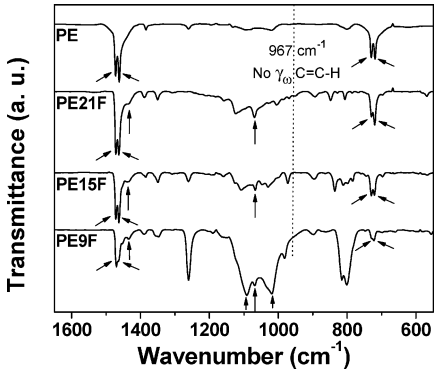

Figure 1. IR of ADMET PE, **PE21F**, **PE15F**, and **PE9F**.

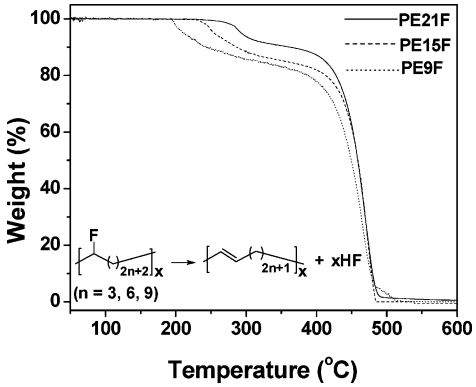

Figure 2. TGA results for **PE21F**, **PE15F**, and **PE9F**.

catalyst, followed directly by exhaustive hydrogenation by diimide reduction[7] to give the polymers **PE9F**, **PE15F**, and **PE21F**. The nomenclature acronym used herein is PE*X*F, which indicates a polyethylene backbone with a fluorine substituent on every *X*th carbon, where $X = 9$, 15, 21. Polymer molecular weights are shown in Table 1 and vary between 7600 and 10 400 g/mol. These molecular weights are characteristic of ADMET polymerizations conducted in solution and are lower than for bulk polymerization conditions,[8] as is typical for polycondensations done in solution when the reaction equilibrium constant is small. The use of solution-based polymerization was necessitated by the rapid solidification of the reaction mixture in the case of the attempted bulk polymerization of monomers **7** and **8** and due to the fact that monomer **9** is a solid.

Primary Structure Characterization. The primary structure of these precise EVF polymers was established using a combination of ^{1}H NMR, ^{13}C NMR, elemental analysis, IR spectroscopy, and TGA (thermogravimetric analysis). The precise structure of the polymers is supported by NMR, and the composition is confirmed by elemental analysis (see Experimental Section). The IR spectra in Figure 1 also provide characteristic information regarding the primary structure of the polymers, where the absence of a peak at 967 cm^{-1} for all three EVF polymers indicates complete hydrogenation, based on the disappearance of the out-of plane olefin C−H wagging vibrational mode.[10] Characteristic peaks are found in several regions of the IR spectra. Vibrational modes associated with C−F stretching are observed at 1069 cm^{-1} for all three EVF polymers.[11] The strong peaks at 1091 and 1019 cm^{-1} in **PE9F** are due to a combination of C−F and C−C stretching.[12] The accentuation of these additional C−F-related modes in **PE9F** is caused by the higher fluorine concentration relative to **PE15F** and **PE21F**. Doublets corresponding to methylene bending modes at ∼1472−1463 cm^{-1} and methylene rocking modes at ∼730−720 cm^{-1} are indicative of methylene sequences in PE analogues with an orthorhombic crystal structure.[13,14] Notice also a shoulder in all of the EVF samples at ∼1434 cm^{-1}, which can be attributed to bending modes for the methylene groups α to the C−F groups.[15]

Thermal Decomposition Analysis. While NMR and IR support the proposed primary structure, TGA results confirm the composition of the polymers. Figure 2 displays the thermal decomposition curves of all three EVF polymers. In all cases, a two-stage decomposition is observed, where the first stage corresponds to the loss of HF and the second stage marks the autocatalytic chain excision and decomposition of the polymer. As was demonstrated in our previous work on ethylene vinyl halide polymers, the mass loss in the first stage quantitatively reflects the halogen content of the polymer.[16] The observed values for mass loss in the first stage are found to be in agreement with the calculated HF content for each of the EVF polymers at 14%, 9%, and 6% for **PE9F**, **PE15F**, and **PE21F**, respectively. Figure 2 also shows that the onset of decomposition for the first stage loss of HF increases with decreasing fluorine content (see also Table 1). Therefore, EVF samples become more stable with increasing content of ethylene units as the labile fluorine content decreases. For comparison, the onset of decomposition for the first stage HF loss in PVF is 455 °C.[17] The significantly higher value, relative to the EVF polymers reported here, can be attributed to the strong dipole−dipole interactions present in PVF, which results in the enhanced stability.

Melting and Crystallization Behavior. Figure 3 shows the cooling and subsequent heating as measured by DSC at a 10 °C/min for **PE9F**, **PE15F**, and **PE21F**. Clearly, under a relatively fast crystallization, the peak melting temperatures (T_m) and crystallization temperatures (T_c) of the three polymers are essentially the same (see Table 1).

There are two factors that contribute to the observed melting behavior in this series. First, because of the relatively low molar mass of these EVF polymers, the observed melting temperatures are depressed by chain-end effects compared to the value of longer chains. For example, under the same crystallization conditions used to obtain the data for the polymer samples in Table 1, the melting temperatures of narrow linear polyethylene fractions in a molecular weight range from 4000 to 12 000 g/mol increase from 127 to 132 °C, respectively (see Experimental Section). It is thus likely that the difference of the observed T_m value for EVFs (124 °C) from the T_m of ADMET linear PE

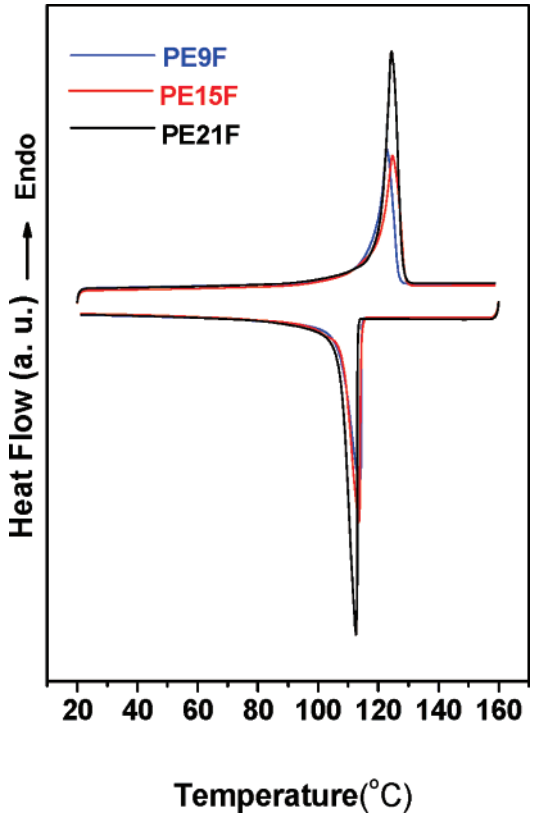

Figure 3. DSC exotherms and endotherms for **PE9F**, **PE15F**, and **PE21F**.

(130 °C) is mainly due to a molar mass effect, with only a small contribution from the presence of F atoms in the orthorhombic lattice at the level of substitution studied. Second, although small, the F is a perturbation in the lattice; therefore, one expects some depression of the melting temperature with increasing fluorine content in precision EVF. However, the melting depression may be small and, under fast crystallization, compensated by the variation of molar mass in the series.

To test this possibility, the melting behavior was also analyzed for isothermally crystallized specimens. Under crystallization conditions closer to the melting point, the shortest molecules remain uncrystallized; thus, the effect of chain ends on melting is minimized. For all isothermal crystallizations (110 °C > T_c < 120 °C), the melting temperatures decrease with increasing content of fluorine, as shown in the Hoffman−Weeks plots of Figure 4. For example, at T_c = 115 °C, the T_m values of **PE9F**, **PE15F**, and **PE21F** are 124.3, 125.7, and 127.7 °C, respectively. These data thus give evidence for the impact of the F unit as a defect, with a higher volume than H, on the thermodynamic melting. Extrapolated to the $T_m = T_c$ line, they yield equilibrium melting temperatures (T_m°) of 127.3 ± 0.7, 132.7 ± 1.8, and 137.6 ± 1.0 °C for **PE9F**, **PE15F**, and **PE21F**, respectively. Also inferred by the inset plot is a linear scaling of the equilibrium melting temperatures with content of fluorine and a T_m° value for the chain free of halogen of ∼144 ±3 °C, in close adherence to the equilibrium value for orthorhombic polyethylene crystals obtained by similar and other extrapolative methods.[18]

From the heat of melting and crystallization the degrees of crystallinity (X_c) were estimated considering uniform F distribution and under the assumption that the heat of fusion per mole of pure crystalline unit is, for the three EVF samples, the same as for polyethylene. The values, listed in Table 1, decrease from 74 to 53% with increasing fluorine content.

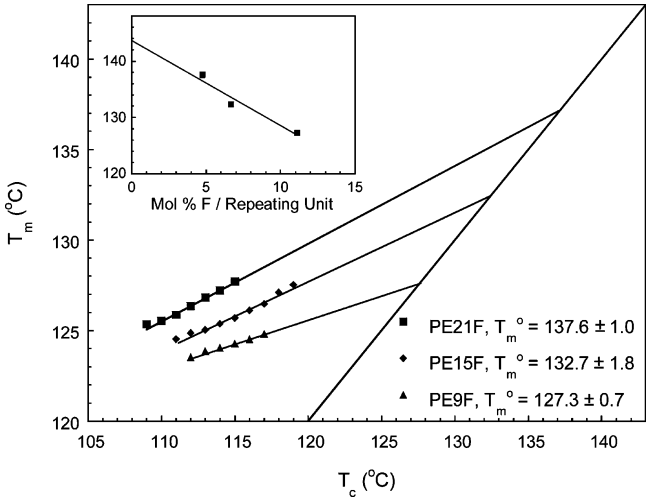

Figure 4. T_m vs T_c of ADMET precision EVF samples.

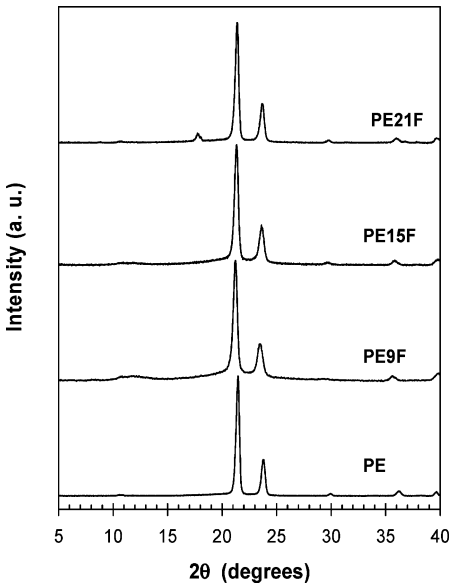

Figure 5. WAXD diffractograms of a narrow linear polyethylene fraction (M_w = 16 500; M_w/M_n = 1.26) and ADMET precision EVF samples slowly cooled from the melt at ∼1 °C/min. The peak at 2θ = 17.9° in **PE21F** belongs to some impurity.

WAXS patterns of precision EVF samples and a low molecular weight linear polyethylene fraction, shown in Figure 5, confirm that the orthorhombic packing of the unsubstituted chain is maintained in the EVF series. Clearly, the linear polyethylene and molecules with precise substitution of fluorine atoms at distances even as close as nine methylenes are isomorphous materials. Small shifts of the two main reflections to lower angles indicate some expansion of the unit cell axes due to the substitution of hydrogen for the larger fluorine atom. In addition, the tacticity cannot be controlled in the ADMET synthesis; thus, the fluorine substitution imparts a defected nature to the precision molecules. Nonetheless, the expansion is not as severe as that rendered by larger halogens (Cl, Br), which crystallize in a less symmetric triclinic packing.[16] Values of the unit cell dimensions, densities of the EVF orthorhombic lattices calculated assuming a uniform fluorine distribution and constant *c*-axis, and degrees of crystallinity (X_c) calculated from the WAXD patterns after peak deconvolution are listed in Table 2.

The decrease in crystallinity with increasing fluorine content parallels the estimated values from heat of fusion and reflects, in reference to polyethylene, the perturbation of the fluorine atom to the development of crystallinity. The similarity between

Table 2. Orthorhombic Lattice Parameters and Crystallinity from WAXD Patterns

sample	$2\theta_{(110)}$ (deg)	$2\theta_{(200)}$ (deg)	a (Å)	b (Å)	c (Å)	V (Å)^3	density (g/cm^3)	$X_{c(WAXS)}$[a]
PE	21.44	23.78	7.484	4.978	2.547	94.894	0.9798	0.88
PE21F	21.38	23.68	7.515	4.989	2.547	95.495	1.0332	0.87
PE15F	21.32	23.62	7.534	5.003	2.547	96.013	1.0514	0.75
PE9F	21.22	23.50	7.572	5.026	2.547	96.929	1.0962	0.62

[a] Degree of crystallinity of linear PE and precision EVF polymers.

Table 3. Structural Parameters of Crystalline Linear PE and EVFs Obtained by SAXS

	Lorentz correction					correlation function			
sample[a]	$X_{c(WAXS)}$ (%)	q_1 (Å^{-1})	q_2 (Å^{-1})	L_1 (Å)[b]	l_{c1} (Å)[c]	L_2 (Å)[d]	l_{a2} (Å)[e]	l_{c2} (Å)[f]	X_{c2} (%)[g]
PE	88	0.026	0.049	242	213	250	40	210	84
PE21F	87	0.029	0.059	214	187	210	45	165	80
PE15F	75	0.039	0.079	160	120	155	48	107	69
PE9F	62	0.041	0.082	153	95	146	49	97	66

[a] Samples slowly cooled from the melt (~2 °C/min). [b] Long spacing ($2\pi/q_1$). [c] Lamellar thickness (L_1X_{WAXS}). [d] Long spacing as first maximum of the correlation function. [e] Amorphous layer thickness from the self-correlation at the first minimum as detailed in Strobl et al.[20] [f] Crystallite thickness ($L_2 - l_{a2}$). [g] Crystallinity within stacks l_{c2}/L_2.

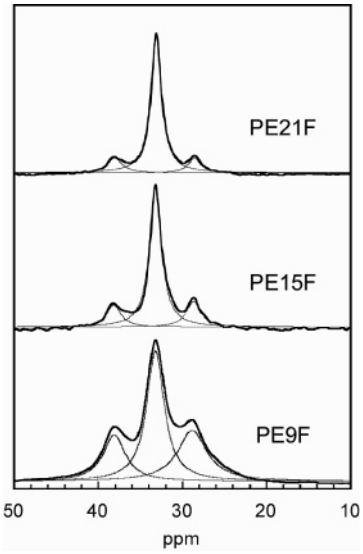

Figure 6. ^{13}C NMR CP/MAS spectra of ADMET precision EVF samples.

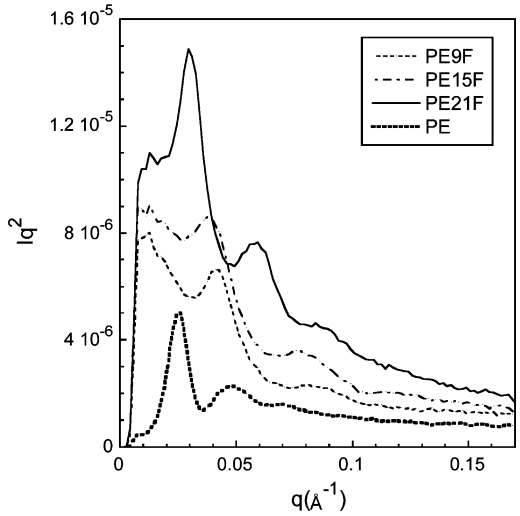

Figure 7. Lorentz-corrected SAXS profiles of a linear polyethylene fraction and ADMET precision EVF samples.

both crystallinities supports the assumption of minor differences in $\Delta H°$ (energy to melt 1 mol of crystalline repeated backbone unit) in the EVF series.

The fact that both melting and crystallization (Figure 3) are marked by sharp transitions suggests, as pointed out in a recent work,[16] a homopolymer crystallization pattern. Evidence for this behavior in the precision EVF series was found in the solid-state ^{13}C NMR spectra in Figure 6. The figure displays CP/MAS spectra of the methylene region acquired under a relatively short contact time and hence are representative of the crystalline regions. The three major resonances observed correspond to α-CH_2 (38.1 ppm), internal CH_2 (33.1 ppm), and β-CH_2 (28.6 ppm), in methylene sequences of identical length flanked by F atoms. The spectra were acquired under high power C−H decoupling; however, because of C−F coupling, the methine region (~95 ppm) was not analyzed. As shown in the figure, the integrated intensity associated with each resonance was obtained from fits with Lorentzian peaks, where the content of fluorine in the crystal corresponds to half of the fractional content of α-CH_2 or β-CH_2 intensities. These values are 4.7 mol % (**PE21F**), 6.6 mol % (**PE15F**), and 10.7 mol % (**PE9F**), in very good agreement with the content of fluorine in the chain that corresponds to 4.8, 6.7, and 11.1 mol %, respectively, for the same polymers. These NMR data demonstrate that the fluorine atom is incorporated into the crystal at a composition equivalent to the overall composition of the polymer. We can then conclude that the precise substitution of a hydrogen for a fluorine atom on each and every 21st, 19th (see ref 16), 15th, or 9th carbon does not change the crystallization pattern of these polymers. In all the series, continuous backbone sequences that include the halogen pack in an *all-trans* conformation along the *c*-axis of the orthorhombic lattice and fold into lamellar crystallites, as suggested by the melting temperatures and the AFM images of melt crystallized specimens (see Supporting Information). Lamellar periodicity is evident, and the apparent crystal thicknesses (~200 Å) are well below the thickness of the extended chain.

A more detailed analysis of the periodicity between lamellar crystallites and amorphous and crystal thicknesses was obtained by small-angle X-ray scattering (SAXS) and from the analysis of the SAXS intensity ($I(q)$) data according to the one-dimensional correlation function.[19] Lorentz-corrected scattering data ($I(q)q^2$ vs q) are given in Figure 7, where two or three diffraction orders are apparent in each SAXS pattern. These data are listed in Table 3. From the ~2.00 ratio of the second and first maxima it is concluded that these peaks correspond to the first-, second-, and third-order reflections from the same structure of lamellae stacks and are not associated with a second population of crystallites. Furthermore, the relatively high peak intensity indicates that precision EVF polymers are highly crystalline and present rather uniform lamellar stack periodicities

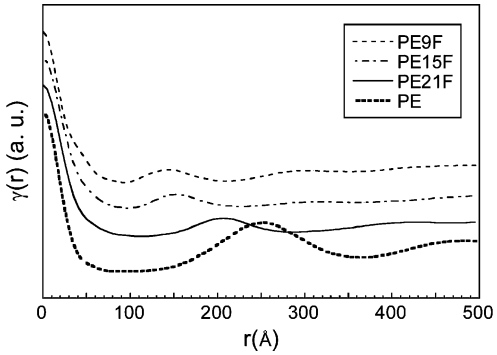

Figure 8. One-dimensional correlation function of a linear polyethylene fraction and ADMET precision EVF samples. The curves are shifted along the *y*-axis for clarity.

(*L*). The variation of *L* and the crystal thickness (l_c) with increasing content of fluorine were first obtained directly from the Lorentz-corrected plots and the crystallinities obtained from WAXS. These data show that both long spacing and crystallite thickness decrease with increasing F content (see Table 3) and suggest that the F atom, as a defect, imposes a restriction to the crystallite thickness. Under the same crystallization mode, the formation of relatively thick crystallites is more restricted in precision EVF chains containing a higher content of fluorine.

The structural parameters of the lamellar stacks obtained from the normalized one-dimensional correlation function, shown in Figure 8, following the method of Strobl and Schneider,[20] are also listed in Table 3. The value of the abscissa at the first maximum corresponds to the long period (L_2), and the thickness of the amorphous layer, l_{a2}, is found from the self-correlation triangle at the first minimum. Identification of this thickness with the amorphous layer is possible for these series due to the much higher estimated values of the crystallite thicknesses observed by AFM. Notice that while the long period decreases in the series from 250 Å for PE to 146 Å for **PE9F**, the thickness of the amorphous regions remains basically constant at ∼45 Å. The thickness of the crystal layer is given by the difference $L_2 - l_{a2}$, listed as l_{c2} in the table. Values of l_{c2} decrease with increasing fluorine and are within 10% of l_{c1} found under the assumption of a model of lamellar stacks covering the complete sample volume, which is implicit in the calculation of l_{c1} as $L_1(X_{c(WAXS)})$. Given the low molecular mass and high crystallinity of PE and the precision EVF polymers studied, regions of amorphous material outside the lamellar stacks are not expected in these samples; indeed, optical microscopy and AFM images corroborate the morphology of crystalline objects and lamellar stacks spanning over the whole film surface (see Supporting Information). This is further evidenced by the similarity between the crystallinity obtained by WAXS and the linear crystallinity or crystallinity within stacks, X_{c2}, found for this series. We should remark that a small fraction of both l_{a2} and l_{c2} include the interfacial region where chains leaving the crystallites become progressively disordered into the amorphous layers. In attempting to calculate the interfacial thickness from experimental SAXS data following for example Ruland's method,[21,22] we found that this calculation gave uncertainties that were too high. However, in reference to previous studies of low molecular weight PEs,[23] the interfacial thickness is estimated to be of 5−8 Å and basically constant in this series. Thus, values of L_2 and l_{c2}, corrected for the interface, will be little affected from those listed in Table 2. Overall, the results from the analysis of the correlation function project a layered structure of alternating amorphous and crystalline regions. The amorphous layers are thin, with a constant thickness of ∼45 Å independent of the content of fluorine in the chain. The crystalline layers are 2−4 times thicker than the amorphous layers, and their thickness decreases from ∼200 to ∼100 Å with increasing fluorine content. For an average molecular weight of 8000 and limiting the chain connectivity between crystallites due to the relatively short chain length, the observed periodicities correspond to molecules that are 2 (PE) to 4 times (PE9F) folded in the semicrystalline solid state of these polymers.

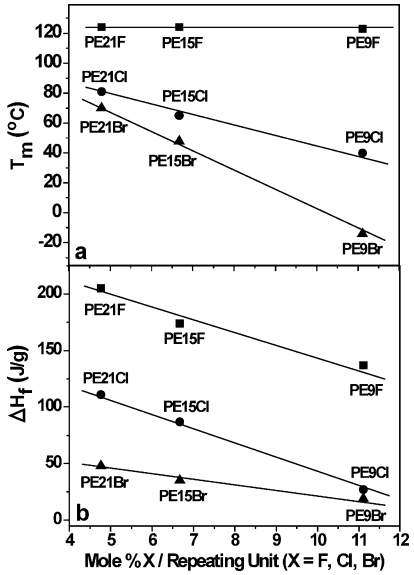

Figure 9. Trends for the variation in observed T_m (a) and ΔH_f (b) vs mol % halogen per repeating unit.

The results for samples crystallized from the melt at 10 °C/min point to an interesting comparison of melting data of EVF with our previous work on precision EVC[5] and EVB[6] polymers of analogous halogen content. Figure 9a depicts the variation of the polymer's melting temperature relative to halogen content and illustrates the influence of the size of halogen substituents. It is observed that for a constant mole percentage of halogen per repeating unit the T_m decreases as the size of the halogen increases. This is in accord with our previously reported comparison of PE19X polymers (where X = F, Cl, and Br)[16] and is attributed to the accommodation of the halogens into the crystal lattice, which serve as defects, lowering the T_m by an amount proportional to the atomic size of the halogen. Notice also in Figure 9a that, for a constant halogen substituent, the apparent T_m decreases as halogen content increases for the case of Cl and Br, but not for F. It is clear that accommodation of greater contents of the larger Cl (van der Waals radius = 1.75 Å) and Br (van der Waals radius = 1.85 Å) atoms into the lattice serves as a defect that changes the crystalline packing of the precision molecules with respect to the unsubstituted chain, thus resulting in a concomitant proportional decrease in T_m. However, the apparent compositionally invariant T_m for the fluorine-containing polymers attests to the fact that the size of the fluorine atom (van der Waals radius = 1.47 Å) is sufficiently small relative to a hydrogen atom (van der Waals radius = 1.2 Å), such that lattice strains due to the inclusion of fluorine are much lower and the orthorhombic packing is maintained. Figure 9b illustrates the variation in ΔH_f relative to halogen size and content for all of the precision EVH polymers. The first observation based on these relationships is that for a constant halogen composition per repeat unit the ΔH_f decreases with increasing halogen size. This result is indicative of the amount of strain that each halogen induces upon incorporation into the crystal lattice as it relates to the amount of energy that must be

added to the system to effect melting. The other observation is that, for the same halogen atom, as the content of halogen increases, the ΔH_f decreases. This has already been explained for the case of the precision EVC[5] and EVB[6] polymers where the incorporation of more halogen atoms into the crystals results in a decrease in crystallinity and in the amount of energy required to disorder the *all-trans* backbone in the crystal lattice. Similarly, for the EVF polymers the percent crystallinity decreases with increasing fluorine content, as calculated from heat of fusion, WAXD, and SAXS.

Conclusions

Herein we have described the synthesis and crystalline structure of a family of precision EVF polymers, which have a F atom on each and every 9th, 15th, and 21st carbon. The precise primary structures and compositions are supported by NMR, IR, TGA, and elemental analysis. Similar to the chlorine and bromine homologues, DSC reveals sharp melting and crystallization transitions characteristic of homopolymers. Crystalline packing at the level of the unit cell indicates that the crystalline state of these precision EVF systems is isomorphous to the linear polyethylene chain. Furthermore, solid-state ^{13}C NMR spectra of the crystalline regions give evidence for a uniform distribution of the F atoms between amorphous and crystalline regions. Hence, as opposed to precision EVC and EVB polymers, accommodation of the smaller F atom in the crystal regions does not change the PE orthorhombic packing. For relatively low molecular mass samples ($M_w \sim 8000$), the crystalline structure is formed of alternating thin amorphous and much thicker crystalline layers, where the chain folds, on average, about 2 (**PE** and **PE21F**), 3 (**PE15F**), or 4 times (**PE9F**). The role of the F atom as a defect in the homopolymer-like crystallization of precision EVF polymers is implicit by the depression of the equilibrium melting temperature, heat of fusion, crystallinity, and crystallite thickness with increasing fluorine content. Nonetheless, while all precision EVH polymers show the characteristics of homopolymers, the size of the halogen has a significant effect on the apparent thermal properties of the polymer.

Experimental Section

Chemicals. Chemicals were purchased from the Aldrich Chemical Co. and used as received unless noted. Grubbs' first-generation ruthenium catalyst, bis(tricyclohexylphosphine)benzylidineruthenium-(IV) dichloride, was purchased from Strem Chemical and stored in an argon-filled drybox prior to use. Methylene chloride and *o*-xylene were distilled over CaH_2.

Linear Polyethylenes. A set of narrow molecular mass fractions of linear polyethylene were obtained from the Societe National Elf Aquitaine (SNPA), France. Their weight-average molecular weight and distribution are the following: 4000 g/mol (1.03), 11 500 g/mol (1.10), and 16 500 g/mol (1.26). These polyethylenes were used to establish the dependence of molar mass on the observed T_m on second melting DSC curves and to obtain a WAXD pattern for the unsubstituted PE chain (16 500 g/mol). An additional PE synthesized via ADMET was also studied. Molecular mass and DSC melting and crystallization data for the latter are listed in Table 1.

Instrumentation. Solution ^1H NMR (300 MHz) and ^{13}C NMR (75 MHz) spectra were recorded on Mercury 300 spectrometer. All chemical shifts for ^1H and ^{13}C NMR were referenced to residual signals from $CDCl_3$ ($^1H = 7.27$ ppm and $^{13}C = 77.23$ ppm) and to residual signals from $C_6D_5CD_3$ ($^1H = 2.09$ ppm and $^{13}C = 137.86$ ppm) with an internal reference TMS 0.03% v/v to internal TMS standard for 0. In all the NMR work the solvents were chloroform-*d* or toluene-d_8 and the temperature was 25 or 80 °C.

High-resolution mass spectral (HRMS) data were obtained on a Finnegan 4500 gas chromatograph/mass spectrometer using the electron ionization (EI) mode. Elemental analyses were carried out by Atlantic Microlabs Inc., Norcross, GA. The GPC measurements for samples were taken on a Waters Associates 150C high-temperature gel permeation chromatograph equipped with three Polymer Laboratories mixed bed Type B columns and an internal DRI detector. The mobile phase was BHT-inhibited 1,2,4-trichlorobenzene (135 °C, flow rate 1.0 mL/min, typical sample concentration 2 mg/mL). IR data were obtained using a Perkin-Elmer Spectrum One FTIR outfitted with a $LiTaO_3$ detector. Measurements were automatically corrected for water and carbon dioxide. Thermogravimetric analysis (TGA) data were obtained with a Perkin-Elmer 7 series thermal analysis system. The TGA samples (2−5 mg) were heated from 50 to 700 °C at 10 °C/min under nitrogen. Melting and crystallizations were obtained at 10 °C/min in a differential scanning calorimeter TA Instruments DSC-Q1000 V9.6 Build 290 under nitrogen flow and calibrated with indium.

$^1H-^{13}C$ cross-polarization combined with MAS (CP/MAS) spectra of the solid polymers were obtained in a Bruker DMX300 spectrometer operating at 75.5 MHz for ^{13}C and at 300.2 MHz for ^1H. The experiments for both types of solid-state NMR were conducted at room temperature using a Bruker solid-state probe for 4 mm rotors under a MAS frequency of 4000 Hz. The small quantities (<100 mg) available for these polymers were placed in the center of the zirconium rotors and the empty spaces filled with fine paper tissue or Teflon tape. The nutation frequencies associated with the ^{13}C and ^1H radio-frequency fields in the CP experiments were 62 kHz for both isotopes. The ^1H nutation frequency applied for decoupling was 83 kHz. Contact times for cross-polarization were 20 μs (**PE21F** and **PE15F**) and 1 ms (**PE9F**). Chemical shifts were measured with respect to tetramethylsilane at 0 ppm as external reference. All peak fit analysis were carried out using the software GRAMS from Galactic Corp.

Wide-angle X-ray diffractograms (WAXD) were collected at room temperature on samples crystallized from the melt at ~1 °C/min using a slit collimated Siemens D-500 diffractometer in a 2θ range between 5° and 40° with a step size of 0.02°. The instrument was calibrated for *d* spacing with a standard polished piece of polycrystalline quartz, and the film thickness was offset using shims.

Small-angle X-ray scattering (SAXS) experiments were performed at $T = 298$ K using a RIGAKU SAXS apparatus equipped with a Bede microsource and a 2D array detector (diameter primary beam $d = 25$ μm, circular cross section). The wavelength of the radiation source was $\lambda = 0.154$ nm (Cu Kα), and the scattering vector, q ($q = 4\pi \sin\theta/\lambda$) (with 2θ denoting the scattering angle), was calibrated using silver behenate standard. The raw intensity was corrected for its value at the pixel location at the beam stop by a linear extrapolation for the calculation of the correlation function. Corrected SAXS intensities were used to obtain the normalized one-dimensional correlation function of the electron density fluctuations perpendicular to the lamellar stacks according to[19]

$$\gamma(r) = \frac{\int_0^\infty q^2 I_c(q) \cos(qr)\, dq}{\int_0^\infty q^2 I_c(q)\, dq}$$

Synthesis. General Procedure for Grignard Reaction. Synthesis of 5-bromopent-1-ene (**1**), 8-bromooct-1-ene (**2**), 11-bromoundec-1-ene (**3**), undeca-1,10-dien-6-ol (**4**), heptadeca-1,16-dien-9-ol (**5**), and tricosa-1,22-dien-12-ol (**6**) was described previously.[6]

General Procedure for Fluorination Reaction. A solution of diethylaminosulfur trifluoride (DAST) (2.0 equiv) in CH_2Cl_2 was cooled to −78 °C, and a solution of the precursor alcohol **4**, **5**, or **6** (1 equiv) in CH_2Cl_2 and dry pyridine (2.5 mL) was added dropwise. The mixture was stirred at this temperature for 2 h and then warmed to room temperature and stirred overnight. At this time water was added and the organic phase was extracted with CH_2Cl_2 and then dried with Na_2SO_4 and then the solvent was removed to give the colorless oils 6-fluoundeca-1,10-diene (**7**) and 9-fluoroheptadeca-1,16-diene (**8**), and the white solid 12-fluorot-

ricosa-1,22-diene (**9**) which were purified by chromatography using 97:3 hexanes:ethyl acetate to give (55−60%) of the product.

6-Fluoroundeca-1,10-diene (7). ^{1}H NMR (300 MHz, $CDCl_3$): δ 5.81 (m, 2H), 5.00 (m, 4H), 4.57−4,41 (dp, 1H), 2.09 (m, 4H), 1.78−1.40 (br, 8H). ^{13}C NMR (75 MHz, $CDCl_3$): δ 138.67, 114.99, 95.51, 93.30, 34.90, 34.63, 33.71, 24.61, 24.55. HRMS calcd for $C_{11}H_{19}F$ $(M + H)^+$, 170.1478; found, 170.1474. Anal. Calcd for $C_{11}H_{19}F$: C, 77.59; H, 11.25; F, 11.16. Found: C, 77.62; H, 11.50; F, 11.01.

9-Fluoroheptadeca-1,16-diene (8). ^{1}H NMR (300 MHz, $CDCl_3$): δ 5.81 (m, 2H), 4.99 (m, 4H), 4.56−4.40 (dp, 1H), 2.06 (m, 4H), 1.69−1.20 (br, 20H). ^{13}C NMR (75 MHz, $CDCl_3$): δ 139.32, 114.42, 95.85, 93.64, 35.51, 35.24, 33.98, 29.58, 29.22, 29.05, 25.34, 25.28. HRMS calcd for $C_{17}H_{31}F$ (M^+), 254.2404; found, 254.2418. Anal. Calcd for $C_{17}H_{31}F$: C, 80.25; H, 12.28; F, 7.47. Found: C, 80.15; H, 12.36; F, 7.41.

12-Fluorotricosa-1,22-diene (9). ^{1}H NMR (300 MHz, $CDCl_3$): δ 5.81 (m, 2H), 4.97 (m, 4H), 4.56−4.40 (dp, 1H), 2.06 (m, 4H), 1.78−1.20 (br, 32H). ^{13}C NMR (75 MHz, $CDCl_3$): δ 139.43, 114.32, 95.89, 93.68, 35.54, 35.27, 34.04, 29.74, 29.69, 29.35, 29.16, 25.39, 25.33. HRMS calcd for $C_{23}H_{43}F$ (M^+), 338.3343; found, 338.3357. Anal. Calcd for $C_{23}H_{43}F$: C, 81.59; H, 12.80; F, 5.61. Found: C, 81.59; H, 12.80; F, 5.43.

General Procedure for Solution Polymerization and Hydrogenation. Monomer and Grubbs' first-generation catalyst (500:1 ratio) were dissolved in toluene under argon and stirred at 45 °C for 5 days. The same amount of catalyst (based on the above ratio) was added into the solution every 24 h. After 5 days the reaction was then stopped, and 50 mL of toluene was added to dissolve the polymer with stirring. The reaction was allowed to cool to room temperature. The polymers were then precipitated by dripping the toluene solution into cold acidic methanol. They were then isolated by filtration and dried.

The unsaturated fluorine containing polymers were then hydrogenated using a modified version of the method described by Hahn[7] by dissolving in dry *o*-xylene under argon and adding 3.3 equiv of *p*-toluenesulfonyl hydrazide (TSH) and 4 equiv of tri-*n*-propylamine (TPA). The solutions were refluxed for 9 h and then cooled to room temperature. The hydrogenated polymer was precipitated into ice-cold methanol and isolated by filtration. The dried polymer was then redissolved in toluene and reprecipitated by dripping into ice-cold acidic methanol. A white solid was collected by filtration and the polymers were isolated in quantitative yield.

PE9F. ^{1}H NMR (300 MHz, toluene-d_8): δ 4.44−4.28 (dp, 1H), 1.75−1.2 (bm, 16H). ^{13}C NMR (75 MHz, toluene-d_8): δ 95.41, 93.16, 36.27, 35.98, 30.32, 30.25, 26.01, 25.95. Anal. Calcd: C, 75.89; H, 12.10; F, 12.00. Found: C, 66.36; H, 11.05; F, 10.77. M_w (GPC vs PE) = 8900 g/mol. PDI = M_w/M_n = 2.0.

PE15F. ^{1}H NMR (300 MHz, toluene-d_8): δ 4.44−4.28 (dp, 1H), 1.75−1.2 (bm, 28H). ^{13}C NMR (75 MHz, toluene-d_8): δ 95.41, 93.17, 36.28, 36.00, 30.48, 30.41, 30.38, 30.00, 26.04, 25.97. Anal. Calcd: C, 78.88; H, 12.80; F, 8.32. Found: C, 74.14; H, 12.37; F, 7.14. M_w (GPC vs PE) = 10 400 g/mol. PDI = M_w/M_n = 2.2.

PE21F. ^{1}H NMR (300 MHz, toluene-d_8): δ 4.44−4.28 (dp, 1H), 1.75−1.2 (bm, 40H). ^{13}C NMR (75 MHz, toluene-d_8): δ 95.41, 93.16, 36.28, 36.00, 30.53, 30.41, 30.38, 26.04, 25.97. Anal. Calcd: C, 80.70; H, 13.22; F, 6.08. Found: C, 79.01; H, 13.17; F, 5.83. M_w (GPC vs PE) = 7600 g/mol. PDI = M_w/M_n = 1.8.

Acknowledgment. Funding of this work by the National Science Foundation, Grants NSF 314110, NSF 0503876, and PREM DMR-0351770, is gratefully acknowledged. We also gratefully acknowledge the generous support from ARO for the acquisition of catalysts, Dr. Lisa Baugh at Exxon-Mobil for obtaining high-temperature GPC data for EVF polymers, the assistance of Dr. E. Lockner of MARTECH (FSU) with X-ray measurements, and the assistance of Dr. R. Fu with solid-state ^{13}C NMR experiments that were carried out at the National High Magnetic Field Laboratory in Tallahassee.

Supporting Information Available: SEC traces for **PE9F**, **PE15F**, and **PE21F** and AFM images for **PE21F** and **PE15F**. This material is available free of charge via the Internet at http://pubs.acs.org.

References and Notes

(1) Scheirs, J. In *Modern Fluoropolymers*; Scheirs, J., Eds.; Wiley: Chichester, 1997; pp 1−69.
(2) Kerbow, D. L. In *Polymeric Materilas Encyclopedia*; Salamone, J. C., Ed.; CRC: Boca Raton, FL, 1996; Vol. 9, pp 6884−6898.
(3) Ameduri, B.; Boutevin, B. *Well-Architectured Fluoropolymers: Synthesis, Properties and Applications*; Elsevier: Amsterdam, 2004; pp 187−230.
(4) Cais, R. E.; Kometani, J. M. *Polymer* **1988**, *29*, 168−172.
(5) Boz, E.; Nemeth, A. J.; Ghiviriga, I.; Jeon, K.; Alamo, R. G.; Wagener, K. B. *Macromolecules* **2007**, *40*, 6545.
(6) Boz, E.; Nemeth, A. J.; Alamo, R. G.; Wagener, K. B. *Adv. Synth. Catal.* **2007**, *349*, 137−141.
(7) Hahn, S. F. *J. Polym. Sci., Part A: Polym. Chem.* **1992**, *30*, 397−408.
(8) Watson, M. D.; Wagener, K. B. *Macromolecules* **2000**, *33*, 3196−3201.
(9) Wunderlich, B. *Macromolecular Physics*; Academic Press: New York, 1973; Vol. 1, pp 401−407.
(10) Sworen, J. C.; Smith, J. A.; Wagener, K. B.; Baugh, L. S.; Rucker, S. P. *J. Am. Chem. Soc.* **2003**, *125*, 2228−2240.
(11) du Toit, F. J.; Sanderson, R. D. *J. Fluorine Chem.* **1999**, *98*, 107−114.
(12) Hong, J. W.; Lando, J. B.; Koenig, J. L.; Chough, S. H.; Krimm, S. *Vib. Spectrosc.* **1992**, *3*, 55−66.
(13) Tashiro, K.; Sasaki, S.; Kobayashi, M. *Macromolecules* **1996**, *29*, 7460−7469.
(14) Ungar, G.; Zeng, X.-B. *Chem. Rev.* **2001**, *101*, 4157−4188.
(15) Bowmer, T. N.; Tonelli, A. E. *J. Polym. Sci., Part B: Polym. Phys.* **1986**, *24*, 1631−1650.
(16) Boz, E.; Wagener, K. B.; Ghosal, A.; Fu, R.; Alamo, R. G. *Macromolecules* **2006**, *39*, 4437−4447.
(17) Impallomeni, G.; Montaudo, G.; Puglisi, C.; Scamporrino, E.; Vitalini, D. *J. Appl. Polym. Sci.* **1986**, *31*, 1269−1274.
(18) Mandelkern, L.; Stack, G. M.; Mathiew, P. J. M. *Anal. Calorim.* **1984**, *5*, 223.
(19) Vonk, C.; Kortleve, G. *Colloid Z. Z. Polym.* **1967**, *19*, 220.
(20) Strobl, G.; Schneider, M. J. *J. Polym. Sci., Polym. Phys. Ed.* **1980**, *18*, 143.
(21) Ruland, W. *Colloid Polym. Sci.* **1977**, *255*, 417.
(22) Koberstein, J. T.; Morra, B.; Stein, R. S. *J. Appl. Crystallogr.* **1980**, *13*, 34.
(23) Mandelkern, L.; Alamo, R. G.; Kennedy, M. A. *Macromolecules* **1990**, *23*, 4721−4723.

MA071403N